The American Journal of Pathology, Vol. 185, No. 1, January 2015

The American Journal of
PATHOLOGY
ajp.amjpathol.org

ANIMAL MODELS

Expression of Human Complement Factor H Prevents Age-Related Macular Degeneration–Like Retina Damage and Kidney Abnormalities in Aged *Cfh* Knockout Mice

Jin-Dong Ding,* Una Kelly,* Michael Landowski,* Christopher B. Toomey,*† Marybeth Groelle,* Chelsey Miller,* Stephanie G. Smith,* Mikael Klingeborn,* Terry Singhapricha,* Haixiang Jiang,‡ Michael M. Frank,‡ and Catherine Bowes Rickman*†

From the Departments of Ophthalmology, Cell Biology,† and Pediatrics,‡ Duke University Medical Center, Durham, North Carolina*

Accepted for publication August 27, 2014.

Address correspondence to Catherine Bowes Rickman, Ph.D., Duke University Medical Center, Box 3802, Durham, NC 27710. E-mail: bowes007@duke.edu.

Complement factor H (CFH) is an important regulatory protein in the alternative pathway of the complement system, and *CFH* polymorphisms increase the genetic risk of age-related macular degeneration dramatically. These same human *CFH* variants have also been associated with dense deposit disease. To mechanistically study the function of CFH in the pathogenesis of these diseases, we created transgenic mouse lines using human *CFH* bacterial artificial chromosomes expressing full-length human *CFH* variants and crossed these to *Cfh* knockout ($Cfh^{-/-}$) mice. Human CFH protein inhibited cleavage of mouse complement component 3 and factor B in plasma and in retinal pigment epithelium/choroid/sclera, establishing that human CFH regulates activation of the mouse alternative pathway. One of the mouse lines, which express relatively higher levels of CFH, demonstrated functional and structural protection of the retina owing to the *Cfh* deletion. Impaired visual function, detected as a deficit in the scotopic electroretinographic response, was improved in this transgenic mouse line compared with $Cfh^{-/-}$ mice, and transgenics had a thicker outer nuclear layer and less sub–retinal pigment epithelium deposit accumulation. In addition, expression of human CFH also completely protected the mice from developing kidney abnormalities associated with loss of CFH. These humanized CFH mice present a valuable model for study of the molecular mechanisms of age-related macular degeneration and dense deposit disease and for testing therapeutic targets. *(Am J Pathol 2015, 185: 29–42; http://dx.doi.org/10.1016/j.ajpath.2014.08.026)*

Age-related macular degeneration (AMD) is a disease that progressively damages the photoreceptors and retinal pigment epithelium (RPE) in the macula, resulting in loss of vision in the center of the visual field. AMD is the leading cause of blindness in the elderly population, affecting approximately 15% of the population older than 70 years of age.[1,2] The earliest clinical signs of AMD are pigmentary changes and the appearance of drusen, focal protein- and lipid-rich extracellular deposits that form between the RPE and the Bruch membrane (BrM). Late-stage AMD is characterized by choroidal neovascularization, geographic atrophy, or both, resulting in irreversible central loss of the choriocapillaris, RPE, and photoreceptors.[3–5] Abnormalities in dark adaptation are often the earliest functional change detected in patients with AMD and reflect impairment of rod photoreceptor function.[6,7]

AMD is a complex disease influenced by a variety of risk factors, including age, which is the greatest.[8] Of the genetic risk factors, a common polymorphism (T1277C) in the complement factor H (*CFH*) gene, resulting in a tyrosine (Y) to histidine (H) substitution at amino acid 402 (H402), has been found to be strongly associated with the

Supported by funding from NIH grants EY019038 (C.B.R.) and P30 EY005722, Edward N. & Della L. Thome Memorial Foundation Award (C.B.R.), and the Foundation Fighting Blindness (C.B.R.).

Disclosure: None declared.

http://dx.doi.org/10.1016/j.ajpath.2014.08.026

development of AMD.[9–12] The same polymorphism has also been linked to dense deposit disease (DDD, also known as membranoproliferative glomerulonephritis type II).[13,14] DDD is a condition that primarily affects kidney function. The symptoms usually appear between ages 5 and 15 years and include hematuria, proteinuria, and nephrotic syndrome.[15,16]

CFH is a major regulator of the alternative pathway (AP) of the complement system. The AP is initiated by complement component 3 (C3) hydrolysis in which a C3 thioester interacts with water to form C3(H_2O). This occurs spontaneously and causes the AP to be continuously active. Uninhibited, C3(H_2O) reacts with complement factor B (FB) to generate C3(H_2O)B, which in the presence of complement factor D is converted to the C3 convertase C3(H_2O)Bb. This conversion allows for further cleavage of C3 to C3b and formation of the C3bBb convertase and initiates the amplification loop. Without negative regulators, this positive feedback loop will quickly deplete all available C3 in the system. CFH is the soluble negative regulator of AP activation. CFH can inhibit formation of the C3 convertase by competing with FB for binding to C3b, accelerate decay of the C3 convertase, and act as a cofactor for factor I–mediated cleavage of C3b.[17]

The complement system is important in defending an organism against foreign invasion by lyzing alien pathogens via the formation of membrane attack complex and signaling debris clearance. However, if dysregulated, the complement system can also attack host cells, causing local inflammation and tissue damage.[18] Available data support the idea that in AMD, the AP is dysregulated owing to CFH malfunction, causing local inflammation and tissue damage in the macular region of the retina. However, the cellular/molecular mechanism(s) for the risk association of CFH in AMD pathogenesis remains unclear. Consistent with a role for CFH in AMD pathogenesis, aged mice lacking CFH ($Cfh^{-/-}$) have an ocular phenotype that shares characteristics of early AMD. These characteristics include decreased electroretinogram (ERG) response, loss of visual acuity, disrupted photoreceptor organization, and structural abnormalities of the BrM.[19,20] These mice also spontaneously develop DDD-like pathologic abnormalities.[21]

To further elucidate the function of CFH in AMD pathogenesis, we generated mice in which full-length human CFH is expressed instead of mouse CFH. Using this mouse model, we tested whether i) human CFH interacts with the mouse AP of the complement system, ii) human CFH protein can rescue the ocular and renal phenotype in $Cfh^{-/-}$ mice, and iii) there are phenotypic differences between mice expressing the normal Y402 or AMD risk–associated H variant of CFH.

Materials and Methods

Generating Bacterial Artificial Chromosome Transgenic Humanized CFH Mice

Mice were housed under normal lighting conditions with 12-hour on/off cycles. The care and treatment of animals were strictly in accordance with the Institutional Animal Care and Use Committee at Duke University (Durham, NC).

The bacterial artificial chromosome (BAC) clone RP11-347L19 contains a 180-kb insert spanning the entire *CFH* gene and two truncated flanking genes (*KCNT2* on the 5′ side and *CFHR3* on the 3′ side). We confirmed by sequencing that the *CFH* gene codes for an H402 form of CFH. To generate the Y402 variant of the humanized *CFH* mice we used BAC clone CTD-2580H3, which has a 132-kb insert in the region spanned by the H402 BAC (UCSC Genome Browser). In collaboration with the Duke Neurotransgenic Laboratory, we generated founder transgenic mice from these BAC clones containing the full-length Y402 [Tg(CTD-2580H3)402Cbr, or *CFH-Y* mice for short] and H402 [Tg(RP11-347L19)301Cbr, or *CFH-H* mice for short] variants of the human *CFH* gene.

The founders were then crossed to C57Bl/6J (C57) mice (The Jackson Laboratory, Bar Harbor, ME). Germline transmission was confirmed by analyzing the genomic DNA of the offspring. Human *CFH*-positive N1 littermates were bred to $Cfh^{-/-}$ mice[21] to generate the *CFH-Y:*$Cfh^{-/-}$ and *CFH-H:*$Cfh^{-/-}$ mouse lines. $Cfh^{-/-}$ mice on a C57 background were obtained from Dr. Glenn Jaffe (Durham, NC) with an material transfer agreement from Imperial College London and permission from Dr. Marina Botto (London, UK). We maintained these two lines by crossing *CFH:*$Cfh^{-/-}$ mice with $Cfh^{-/-}$ mice. The $Cfh^{-/-}$ littermates served as controls. Animals used in this study were crossed to $Cfh^{-/-}$ for more than six generations. We also mated *CFH-H:*$Cfh^{-/-}$ mice together to generate a line of homozygous *CFH-H* transgenic mice (*CFH-HH:*$Cfh^{-/-}$), bearing in mind that this might interrupt an endogenous gene important for normal development.[22] We confirmed that none of the mice carry the *rd8* mutation.[23]

Table 1 Numbers of Mice Used for Each Class of Experiments

							Kidney histology	
Genotype	Real-time PCR	Biochemistry	IHC analysis	ERG	Retina histology	Retina TEM	Aged 2 years	Aged 8 months
C57		6	4	4	9	9	4	3
Cfh$^{-/-}$		6	3	6	11	13	4	5
CFH-Y:Cfh$^{-/-}$	3	9	3	11	7	10	5	4
CFH-H:Cfh$^{-/-}$	3	9	3	13	9	10	5	3
CFH-HH:Cfh$^{-/-}$		4			4			4

ERG, electroretinogram; IHC, immunohistochemical; TEM, transmission electron microscopy.

The ocular and renal phenotypes of 2-year-old C57, *Cfh*$^{-/-}$, *CFH-Y:Cfh*$^{-/-}$, and *CFH-H:Cfh*$^{-/-}$ mice were studied using biochemical, histologic, ultrastructural, and ERG methods. Tissue mRNA and real-time quantitative PCR (qPCR) studies were conducted on 3-month-old *CFH-Y:Cfh*$^{-/-}$ and *CFH-H:Cfh*$^{-/-}$ mice. The renal histologic composition was also investigated in 8-month-old mice of these four genotypes and *CFH-HH:Cfh*$^{-/-}$ mice. The numbers of mice for each class of experiments are summarized in Table 1.

Genotyping of Mice

Transgenic mouse lines were identified and maintained by PCR using DNA isolated from the tail. A human *CFH* gene fragment was amplified using 5′-GCAAACCTTTGTTAG-TAACTTTAG-3′ (forward) and 5′-GTATTGTGTTCAAA-TTCTTTTACTG-3′ (reverse) primers, resulting in a 550-bp amplicon. For the *Cfh*$^{-/-}$ sequence, there is an absence of the 462-bp product amplified in the normal C57 using 5′-GCTACCTACAAATGCCGCCCTG-3′ (forward) and 5′-TCCAACTGCCAGCCTAAAGGAC-3′ (reverse) primers and the presence of a 200-bp amplicon with 5′-GAGGC-TATTCGGCTATGACTG-3′ (forward) and 5′-CCACGA-TAGCCGCGCTGCCTCG-3′ (reverse). Primers used to determine the presence of the *rd8* mutation were 5′-GCC-CCTGTTTGCATGGAGGAAACTTGGAAGACAGCTA-CAGTTCTTCTG-3′ (forward) and 5′-GCCCCATTTG-CACACTGATGAC-3′ (reverse), which would produce an amplicon of 244 bp if the mutation was present; using 5′-GTGAAGACAGCTACAGTTCTGATC-3′ (forward) with 5′-GCCCCATTTGCACACTGATGAC-3′ (reverse), no 220-bp amplicon would be seen if the mutation was present. To genotype the *CFH-HH:Cfh*$^{-/-}$, *CFH-H:Cfh*$^{-/-}$, and *Cfh*$^{-/-}$ mice obtained through the *CFH-H:Cfh*$^{-/-}$ and *CFH-H:Cfh*$^{-/-}$ crosses, we used a qBiomarker copy number variant PCR assay (Qiagen Inc., Valencia, CA) specific for the intron and exon boundary of exon 2 of *CFH* to determine the relative genomic copy number of *CFH*. qPCR reactions were run in duplicate (iCycler; Bio-Rad Laboratories, Hercules, CA) at 95°C for 10 minutes, followed by 40 cycles at 95°C for 15 seconds and 60°C for 60 seconds (qBiomarker SYBR fluor mastermix; Qiagen Inc.). Genomic *CFH* copies were normalized to mouse *Gapdh* (RT^2 PCR primer set *Gapdh*; Qiagen Inc.) using the $2^{-\Delta\Delta C_T}$ method.[24] *CFH-HH:Cfh*$^{-/-}$ mice have approximately twice the number of genomic *CFH* copies compared with *CFH-H:Cfh*$^{-/-}$ mice (Supplemental Figure S1).

Quantitative RT-PCR

Mice were euthanized with carbon dioxide. Brain, eye, intestine, heart, kidney, liver, lung, gut, and spleen were collected from three *CFH-Y:Cfh*$^{-/-}$ and three *CFH-H:Cfh*$^{-/-}$ mice. Total RNA was extracted using an RNeasy lipid tissue mini kit (Qiagen Inc.) according to the manufacturer's instructions. cDNA was synthesized from total RNA (SuperScript VILO cDNA synthesis kit; Invitrogen, Grand Island, NY). qPCR reactions were run in triplicate (iCycler) at 95°C for 3 minutes, followed by 40 cycles at 95°C for 10 seconds and 60°C for 20 seconds, then 72°C for 15 seconds (EXPRESS SYBR GreenER qPCR supermix universal kit; Invitrogen). Each reaction contained 25 ng of cDNA, 200 nmol/L each primer, and 10 μL of qPCR supermix in 25 μL of total volume. Relative CFH mRNA expression was normalized to an endogenous reference gene, *GAPDH*, for each tissue using the quantitative $2^{-\Delta\Delta C_T}$ method.[24] The primers used were 5′-TGTGAGGGTGGTTTCAGGAT-3′ (forward) and 5′-CCATGAGAAATCTCAGGTGGA-3′ (reverse) for *CFH* and 5′-AGGTCGGTGTGAACGGAT-TTG-3′ (forward) and 5′-TGTAGACCATGTAGTTGAGG-TCA-3′ (reverse) for GAPDH.

Western Blot Analysis for Quantitation of CFH, C3, C3b, and FB in Plasma and Tissue Lysates

Mice were euthanized with carbon dioxide, the chest was cut open, and blood was collected from the heart into EDTA tubes (BD Microtainer; BD Biosciences, Franklin Lakes, NJ) at 4°C. Tubes were centrifuged for 5 minutes at 1500 rpm, and plasma was collected. RPE/choroid/sclera was dissected from each mouse eye. Radioimmunoprecipitation assay buffer (80 μL) with protease inhibitors (cOmplete, mini, EDTA-free; Roche Diagnostics GmbH, Mannheim, Germany) was added to each eyecup and was homogenized using a battery-operated microgrinder from Argos Technologies (Elgin, IL). After sitting on ice for 30 minutes with vortexing every 10 minutes, the lysates were centrifuged at 14,000 rpm for 15 minutes at 4°C, and the supernatant was transferred to a new tube. Protein estimation was performed using a bicinchoninic acid protein assay kit (Pierce Biotechnology, Rockford, IL), and 5 μg of total protein for CFH and 20 μg of total protein for C3 and FB were used for Western blot analyses.

The polyclonal goat anti-human CFH antibody (Quidel Corp., San Diego, CA) recognized human and mouse CFH with significantly different affinity. Therefore, mouse CFH standards were prepared by purifying CFH from C57 plasma, as previously described, and were quantified using human CFH standards (CompTech, Tyler, TX) on Coomassie-stained gels using a standard curve of 100 to 600 ng of CFH per well.[25] We also established that the antibody identically recognized human CFH-H and CFH-Y purified from human plasma (obtained from homozygous individuals) and mouse plasma of *CFH-Y:Cfh*$^{-/-}$ and *CFH-H:Cfh*$^{-/-}$ mice. We quantified the isolated human CFH from these sources on Coomasie-stained gels and compared 8, 32, and 64 pg of each CFH on a Western blot analysis (Supplemental Figure S2). Protein levels of mouse CFH in mouse plasma were measured using mouse CFH standards that were loaded onto the gels with C57 plasma, and human CFH standards were loaded onto the gels measuring the human CFH concentration in the *CFH-Y:Cfh*$^{-/-}$ and *CFH-H:Cfh*$^{-/-}$ mouse plasma. Plasma

samples were diluted 1:500 in 5% sample buffer, then 1.5 μL of this dilution for CFH and 20 μL for C3, C3b, and FB were run, nonreduced on 10% Bis-Tris Criterion XT gels in a 3-(N-morpholino)propanesulfonic acid (MOPS) buffer, transferred to nitrocellulose, blocked with 10% nonfat milk for C3 or 4% bovine serum albumin for CFH and FB, then probed with goat anti-CFH, anti-FB (Kent Laboratories, Bellingham, WA), or rabbit anti-C3d (Dako, Carpinteria, CA). Subsequent incubation with horseradish peroxidase–conjugated anti-goat or anti-rabbit secondary antibodies (Jackson ImmunoResearch Laboratories, West Grove, PA) was followed by detection with ECL Plus reagent (Pierce Biotechnology). The images were scanned and the densities measured by ImageJ software version 1.46 (NIH, Bethesda, MD).

Hemolytic Assay for the Functional Measurement of Complement Activity in Mouse Plasma

Normally, the functional activity of complement is measured by the CH50 hemolytic assay. However, because of the small volumes of mouse blood and the low CH50 values obtained, this assay is difficult to perform on mouse plasma. The assay described herein measures functional, intact mouse C3 based on the ability of mouse plasma to provide C3 to reconstitute C3-depleted human serum in the lysis of antibody-sensitized sheep erythrocytes.

Preparation of Sensitized Sheep Erythrocytes

To sheep erythrocytes (EAs; Lampire Biological Products, Pipersville, PA) at 1×10^9/mL in $GVBS^{++}$ (Veronal-buffered saline, 0.1% gelatin, 0.15 mmol/L $CaCl_2$, and 1.0 mmol/L $MgCl_2$) was added an equal volume of diluted rabbit anti-sheep erythrocyte IgG, incubated at 30°C for 15 minutes, then centrifuged and washed in $GVBS^{++}$.

C3 Hemolytic Activity

Keeping everything on ice, six doubling dilutions of mouse plasma were made in $GVBS^{++}$ starting with 1:20 for *Cfh*$^{-/-}$, *CFH-Y:Cfh*$^{-/-}$, and *CFH-H:Cfh*$^{-/-}$ mouse plasma and 1:50 for C57 mouse plasma. Two hundred microliters of each dilution was added to EAs (1×10^8) in 200 μL of $GVBS^{++}$, then 100 μL of a 1:20 dilution of C3-depleted human serum was added. The reaction mixture was incubated at 37°C in a shaking water bath for 1 hour, then 500 μL of ice-cold EDTA-GVBS was added to stop the reaction. The tubes were spun at 3000 rpm for 5 minutes, and OD was measured at 412 nm. The reciprocal of the dilution at which 50% hemolysis was achieved gave the hemolytic units for that sample. One hundred percent hemolysis was determined by EAs (1×10^8) in 200 μL of $GVBS^{++}$ with 300 μL of H_2O minus the hemolysis due to EAs (1×10^8) in 200 μL of $GVBS^{++}$ plus 100 μL of a 1:20 dilution of C3-depleted human serum plus 200 μL of $GVBS^{++}$.

Immunofluorescence

Mice were deeply anesthetized using a ketamine and xylazine mixture and were perfused transcardially with phosphate-buffered saline briefly, followed by 4% paraformaldehyde in 0.1 mol/L phosphate buffer (PB), pH 7.4. Eyes and kidneys were postfixed in the same fixative overnight and were cut using a vibratome into approximately 50-μm-thick sections. Free-floating sections were blocked with 10% normal donkey serum and then were incubated overnight with the following primary antibodies: goat anti-human CFH (dilution 1:100) (A312; Quidel Corp.) or goat anti-mouse C3 (dilution 1:500) (#55444; MP Biomedicals, Santa Ana, CA), followed by Alexa Fluor–conjugated donkey anti-goat secondary antibody (dilution 1:500) (Invitrogen) and Hoechst 33258 (Invitrogen) to counterstain the nuclei. Tyramide signal amplification was used for rat anti-mouse C3b/iC3b/C3c antibody (clone 2/11; Hycult Biotech, Uden, the Netherlands) to enhance the signal. Images were acquired using a Leica SP5 laser scanning confocal microscope (Leica Microsystems Inc., Buffalo Grove, IL).

ERG

Mice were dark adapted overnight, their pupils were dilated with 0.5% tropicamide and 1.25% phenylephrine, and they were anesthetized with a mixture of ketamine (100 mg/kg) and xylazine (10 mg/kg). Scotopic ERGs were recorded using an Espion E^2 system (Diagnosys LLC, Lowell, MA) at flash intensities of 2.5×10^{-5}, 5×10^{-5}, 5×10^{-4}, 5×10^{-3}, 0.05, 0.5, 5, 50, and 500 cd·s/m^2, as previously described.[26,27] Low-pass frequency filtering of 50 Hz was applied to remove oscillatory potentials and noise. Amplitudes of b-waves were calculated from the bottom of the a-wave response to the peak of the b-wave. The data points from the b-wave stimulus-response curves were fitted according to a previously published equation[28] using the least-square fitting procedure in OriginPro 9.0 software (OriginLab, Northampton, MA).

Retina Histologic Analysis

Mice were deeply anesthetized using a ketamine and xylazine mixture and were perfused transcardially with phosphate-buffered saline briefly, followed by fixative (2% paraformaldehyde and 2% glutaraldehyde in 0.1 mol/L PB, pH 7.4). Eyes were enucleated and fixed in the same fixative overnight. Posterior eyes were osmicated, dehydrated through graded ethanol, infiltrated, and embedded in a mixture of epoxy and Spurr resins. Semithin sections of 0.5 μm were cut, mounted, and stained with toluidine blue. Sections were viewed and photographed under a light microscope (Carl Zeiss MicroImaging GmbH, Jena, Germany). The outer nuclear layer (ONL) thickness was measured along the superior-inferior meridian of the eye at the level of the optic nerve using ImageJ software.

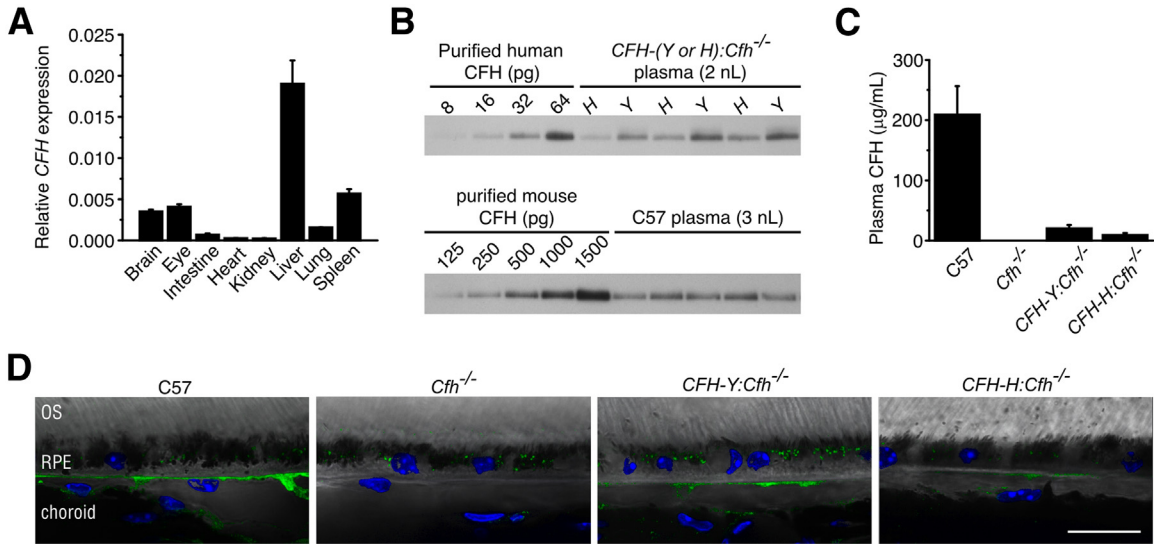

Figure 1 Human *CFH* gene and CFH protein are expressed in mouse tissue. **A:** Relative expression of *CFH* to *GAPDH* was calculated using $2^{-\Delta\Delta C_T}$. CFH mRNA was widely expressed, with the highest expression in the liver, followed by the spleen, eye, and brain. **B:** CFH immunoblots quantifying CFH in mouse plasma. Standard curve of purified human CFH and human CFH protein in *CFH-Y:Cfh*$^{-/-}$ and *CFH-H:Cfh*$^{-/-}$ mouse plasmas using anti-human CFH antibody. Two microliters of a 1:1000 dilution of plasma per well. The same antibody also detected mouse CFH protein in C56Bl/6J (C57) mouse plasma. Note that the affinity is much lower for mouse CFH. **C:** Plasma CFH protein concentrations calculated from Western blots shown in **B**. The circulating concentration of human CFH is much lower compared with that of C57 mouse CFH levels ($n = 3$ per genotype). The result was confirmed in three separate experiments. **D:** Immunofluorescence localization of CFH on retinal pigment epithelium (RPE)/choroid sections of 2-year-old mice. Strong labeling of CFH is found in the choriocapillaris of C57 eye. Staining is absent in *Cfh*$^{-/-}$ mice. Weak staining is present in the choriocapillaris of *CFH-Y:Cfh*$^{-/-}$ and *CFH-H:Cfh*$^{-/-}$ mice. Puncta inside the RPE are lipofuscin autofluorescence. Data are given as means ± SD. Scale bar = 20 µm. OS, outer segment.

Retina TEM and Basal Deposit Sampling

For transmission electron microscopy (TEM), approximately 200-µm-thick vibratome sections in the center of the eye through the optic nerve head were osmicated, stained *en bloc* with uranyl acetate, dehydrated, and embedded in a mixture of epoxy and Spurr resins. Each embedded section was then divided into two parts on each side of the optic nerve head (Supplemental Figure S3A). Thin sections of 60 to 80 nm were cut from each region spanning 70% to 80% of the total length of the retina from the optic nerve toward the ora serrata, collected onto 400-mesh thin-bar copper grids (T400-Cu; Electron Microscopy Sciences, Hatfield, PA), and stained with uranyl acetate and Sato's lead. Sections were viewed using a Tecnai G^2 electron microscope (FEI, Hillsboro, OR). Images containing the basal RPE and BrM were taken on the parts of the section adjacent to the grid's bar throughout the length of the retina. For each image, the thickness of the deposits was measured from the central elastin layer of the BrM to the top of the deposit near the edges of the image (Supplemental Figure S3) using ImageJ software. Cumulative distribution of deposit thickness was plotted using OriginPro 9.0 software. A nonparametric Kolmogorov-Smirnov test was used to compare the differences between the distribution curves.

Kidney Histologic Analysis and Glomerular Grading

Kidneys from 2% paraformaldehyde– and 2% glutaraldehyde–perfused mice were postfixed overnight in the same fixative before being dehydrated and embedded in paraffin. Ten-micron sections were cut and stained with periodic acid–Schiff reagent. Glomerular histologic appearance was graded using the grading system described previously[21] in which grade 0 was normal; grade I, segmental hypercellularity in 10% to 25% of the glomeruli; grade II, hypercellularity involving >50% of the glomerular tuft in >25% to 50% of the glomeruli; grade III, hypercellularity involving >50% of the glomerular tuft in >50% to 75% of the glomeruli; and grade IV (the most severe), glomerular hypercellularity in >75% or crescents in >25% of the glomeruli. For scoring, 50 glomeruli per section were analyzed by masked investigators (J.-D.D., C.M.). Semithin plastic sections and TEM sections were processed the same way as the retina tissue.

Results

Generating Human CFH Transgenic Mice

We generated nine founder transgenic mice using full-length BACs containing the Y402 ($n = 5$) and H402 ($n = 4$) variants of human *CFH*. These founders were then crossed to C57 mice. Germline transmission was confirmed in all founder lines by analyzing the genomic DNA of the N1 offspring. However, mRNA for human CFH was found in only seven lines (five for H402 and two for Y402). These seven lines were then crossed to *Cfh*$^{-/-}$ mice.[21] Using qPCR analysis, we observed the highest levels of human CFH mRNA in the liver, although other tissues, including the eye, also express the transcript (Figure 1A).

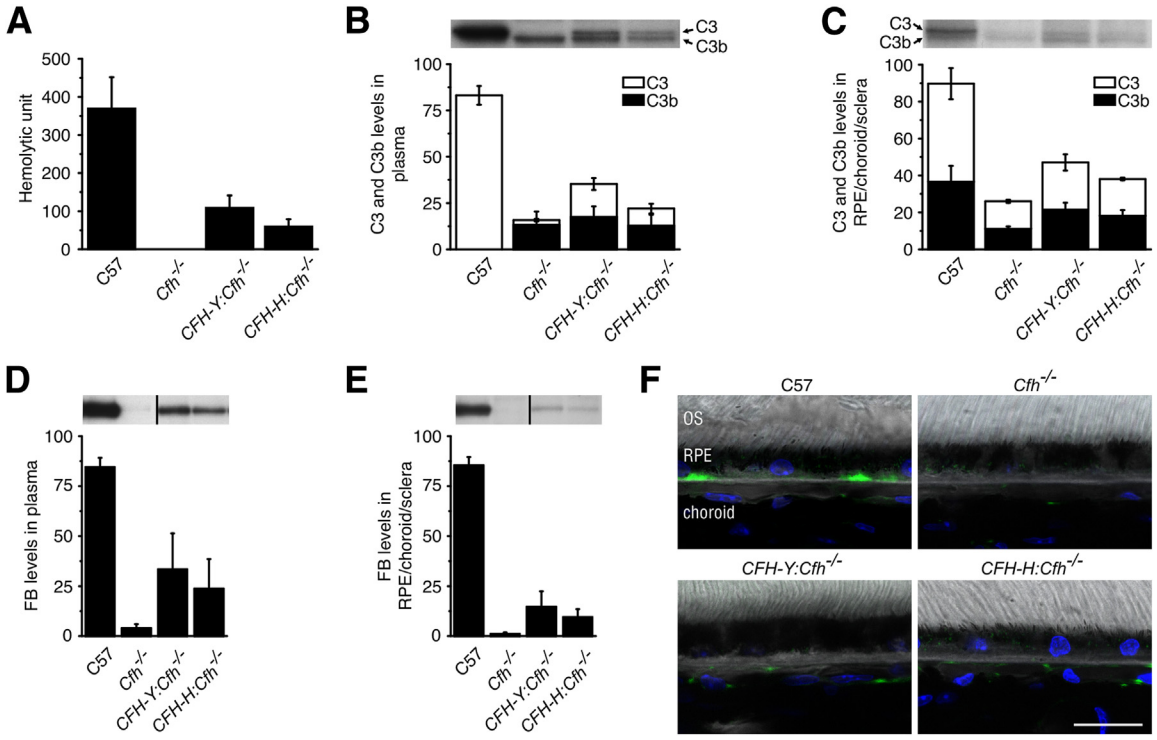

Figure 2 Human CFH protein inhibits activation of the mouse AP of the complement system *in vivo*. **A:** Mouse plasma hemolytic C3 activity. The C57 mouse had the highest hemolytic activity, whereas no hemolysis was detected using $Cfh^{-/-}$ mouse plasma. *CFH-Y:*$Cfh^{-/-}$ and *CFH-H:*$Cfh^{-/-}$ mice had approximately 30% and 15%, respectively, of the C57 hemolytic activity. **B:** Western blot analysis of C3 in the plasma. All the C3 in C57 mice was uncleaved. *CFH-Y:*$Cfh^{-/-}$ and *CFH-H:*$Cfh^{-/-}$ mice showed approximately equal amounts of C3 and C3b, although there was significantly more of both in *CFH-Y:*$Cfh^{-/-}$ mice, and only C3b could be readily detected in $Cfh^{-/-}$ mice. **C:** Western blot analysis of C3 in the RPE/BrM/choroid/sclera. There was a smaller difference in the relative amounts of C3 and C3b between the genotypes in the tissue, and a small amount of intact C3 was detected in $Cfh^{-/-}$ mice, suggesting that inhibitors other than CFH act on locally produced C3. FB levels in plasma (**D**) and in the RPE/choroid/sclera (**E**) are shown. Western blot analysis of FB in plasma and tissue showing that virtually all the FB has been consumed in the plasma and tissue in $Cfh^{-/-}$ mice, whereas there is some intact FB in *CFH-Y:*$Cfh^{-/-}$ and *CFH-H:*$Cfh^{-/-}$ mice, although this is significantly less than that found in C57 mice. **F:** Confocal immunofluorescence images depict immunolocalization of C3b/iC3b/C3c (green) in mouse eyes. In C57 mice, C3b/iC3b/C3c immunolabeling was present in dense patches along the basal side of the retinal pigment epithelium (RPE)/BrM and in the choriocapillaris. Immunolabeling for C3b/iC3b/C3c was totally absent in $Cfh^{-/-}$ mice. In *CFH-Y:*$Cfh^{-/-}$ and *CFH-H:*$Cfh^{-/-}$ retinas, C3b/iC3b/C3c staining was seen only in the choriocapillaris. Data are given as means ± SD. Scale bar = 20 μm. OS, outer segment.

Significant amounts of human CFH protein could be detected in the plasma of only two of the lines crossed to $Cfh^{-/-}$ mice, one expressing the H402 form (*CFH-H:*$Cfh^{-/-}$) and the other the Y402 form (*CFH-Y:*$Cfh^{-/-}$). We confirmed the amino acid identity at position 402 in these mice by matrix assisted laser desorption ionization tandem time-of-flight analyzer (MALDI-TOF-TOF) as previously described.[29] Quantification of means ± SD CFH concentrations in these two mouse lines revealed that there is twofold more CFH protein in *CFH-Y:*$Cfh^{-/-}$ plasma (20.3 ± 5.8 μg/mL) than in *CFH-H:*$Cfh^{-/-}$ plasma (9.2 ± 3.5 μg/mL; $P < 0.001$) (Figure 1, B and C). For comparison, the means ± SD plasma concentration of mouse CFH protein in C57 mice is 209 ± 47 μg/mL, 10 to 20 times higher than human CFH in the transgenic lines (Figure 1, B and C). In the back of the eye, CFH mainly localized to the choriocapillaris, as shown by immunofluorescence (Figure 1D). Staining is strong in C57 mice but weaker in *CFH* transgenic mice. Staining was absent in $Cfh^{-/-}$ mice (Figure 1D).

Human CFH Interacts with the Mouse AP

To address whether the human CFH protein can substitute for the mouse CFH and regulate the mouse AP, we tested the impact of human CFH expression on inhibition of the cleavage of C3 *in vivo*. We developed a sensitive and quantitative hemolytic assay for the measurement of intact, fully functional C3 in mouse serum. The means ± SD C3 hemolytic activity in C57 mouse serum was 369 ± 83 U/mL but was not detectable in the $Cfh^{-/-}$ mouse, indicating that all the C3 in the $Cfh^{-/-}$ mice was already cleaved (Figure 2A). Means ± SD hemolysis was readily measured in the serum of the two humanized CFH mouse lines (*CFH-Y:*$Cfh^{-/-}$: 108 ± 32; *CFH-H:*$Cfh^{-/-}$: 60 ± 19), demonstrating that human CFH inhibits C3 cleavage (Figure 2A). The amount of hemolysis measured in *CFH-Y:*$Cfh^{-/-}$ mice was significantly higher than in *CFH-H:*$Cfh^{-/-}$ animals ($P < 0.001$; Student's *t*-test), consistent with the higher level of CFH expression in *CFH-Y:*$Cfh^{-/-}$ mice. Western blot analyses of C3 in plasma from $Cfh^{-/-}$ mice confirmed the absence of

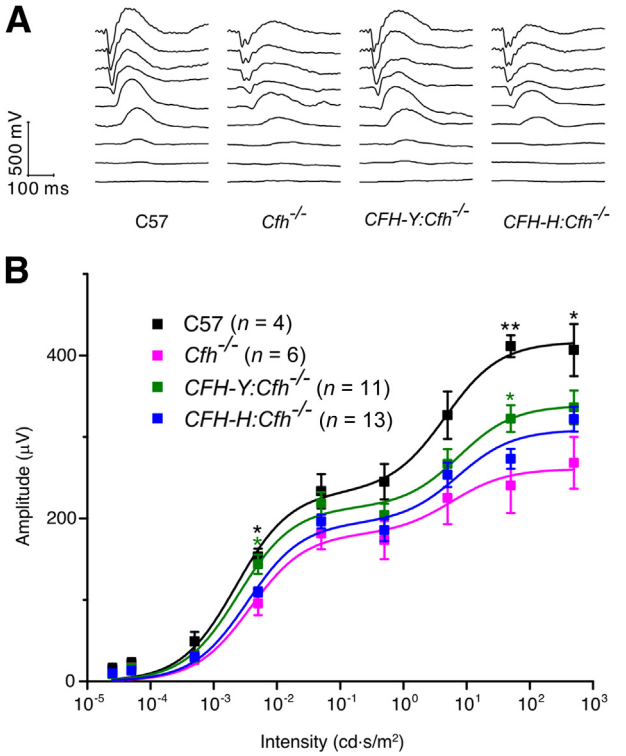

Figure 3 The human *CFH* transgene partially rescues the visual function loss caused by the *Cfh* gene deletion. **A:** Representative traces of the scotopic ERG flash response. **B:** Scotopic ERG flash responses. Stimulus-response curves of b-wave amplitudes. Baseline ERGs obtained from normal C57BL/6J (C57) controls (black) and affected $Cfh^{-/-}$ animals (pink). The scotopic ERG b-wave amplitudes were partially preserved in *CFH-Y*:$Cfh^{-/-}$ mice but not in *CFH-H*:$Cfh^{-/-}$ mice. Data are given as means ± SEM. $^{*}P < 0.05$, $^{**}P < 0.01$ (Student's *t*-test) compared with $Cfh^{-/-}$ animals.

detectable intact C3, with only the lower C3b band being present (Figure 2B).

Human CFH inhibition of C3 hydrolysis *in vivo* was also observed in the RPE/choroid/sclera tissue by Western blot analysis. Two tightly migrating bands were identified on the blot as C3 and C3b. The amounts of C3 and C3b were greatly reduced in $Cfh^{-/-}$ mice compared with C57 mice, but not completely absent, suggesting that inhibitors other than CFH are acting at the tissue level. In *CFH-Y*:$Cfh^{-/-}$ and *CFH-H*:$Cfh^{-/-}$ RPE/choroid/sclera, the levels of C3 and C3b were higher than those in $Cfh^{-/-}$ mice, demonstrating that human CFH has an inhibitory effect at the tissue site (Figure 2C).

We also measured the amount of FB in the plasma (Figure 2D) and the RPE/choroid/sclera (Figure 2E) of *CFH-Y*:$Cfh^{-/-}$, *CFH-H*:$Cfh^{-/-}$, and $Cfh^{-/-}$ mice. On activation of the AP, FB binds to C3b and is subsequently cleaved by complement factor D to form the AP convertase C3bBb. Compared with C57 mice, FB in $Cfh^{-/-}$ mice was nearly completely consumed as a result of uncontrolled activation of the AP. In contrast, FB levels were partially restored in humanized mice, indicating that AP activation was comparatively inhibited (Figure 2, D and E).

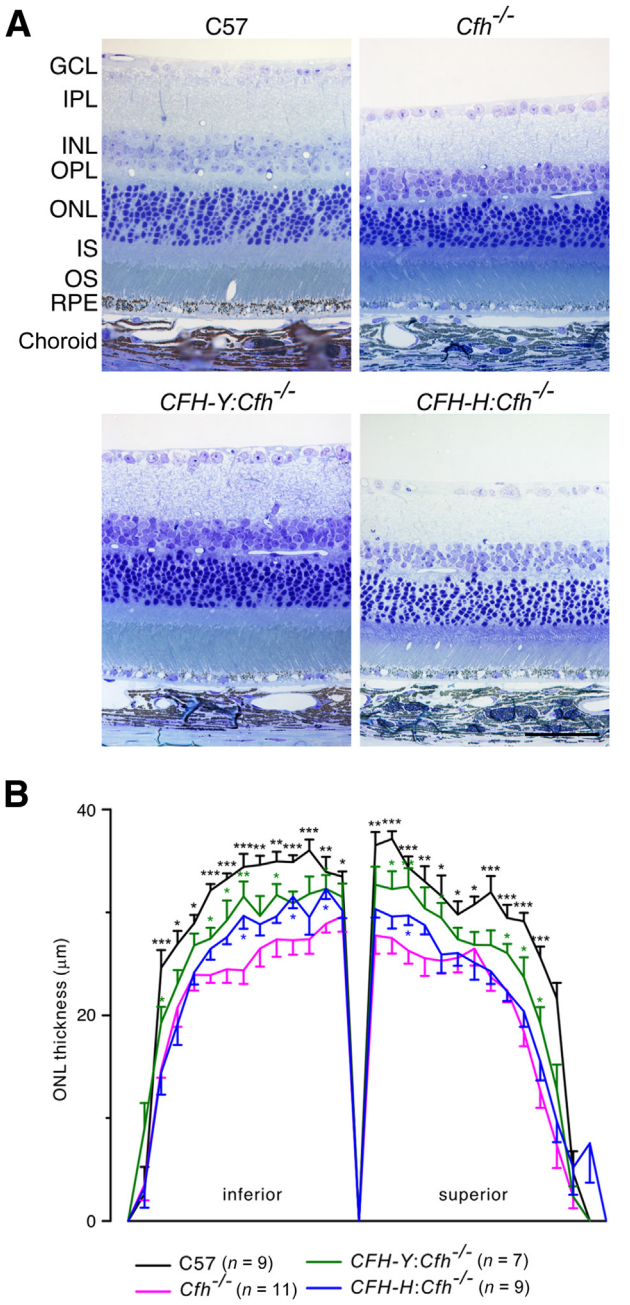

Figure 4 The human *CFH* transgene protects against photoreceptor loss caused by the *Cfh* gene knockout. **A:** Representative micrographs of the retina of the four mouse lines. **B:** The plot of ONL thickness versus eccentricity (spider plot) from the optic nerve shows that the ONL in the C57 retina was significantly thicker than the $Cfh^{-/-}$ ONL. The *CFH-Y*:$Cfh^{-/-}$ ONL was also thicker than the $Cfh^{-/-}$ ONL, indicating that photoreceptor degeneration is partially protected. There was a slightly thicker ONL of *CFH-H*:$Cfh^{-/-}$ mice in the inferior region. Data are given as means ± SEM. $^{*}P < 0.05$, $^{**}P < 0.01$, and $^{***}P < 0.001$ (Student *t*-test). Scale bar = 50 µm. GCL, ganglion cell layer; INL, inner nuclear layer; IPL, inner plexiform layer; IS, inner segment; ONL, outer nuclear layer; OPL, outer plexiform layer; OS, outer segment; RPE, retinal pigment epithelium.

Immunofluorescence of C3b/iC3b/C3c on retina sections was consistent with the biochemical results. In C57 mice, C3b/iC3b/C3c immunolabeling was detected in dense patches along the basal RPE/BrM and in the

choriocapillaris. Immunolabeling for C3b was totally absent in *Cfh*$^{-/-}$ mice. In *CFH-Y:Cfh*$^{-/-}$ and *CFH-H:Cfh*$^{-/-}$ retinas, weaker C3b/iC3b/C3c staining was present in the choriocapillaris but not in the basal RPE/BrM (Figure 2F).

Human CFH Partially Restores Retinal Visual Function and Inhibits Photoreceptor Loss

We next assessed visual function of the retinas of these mice using scotopic ERG, which primarily represents rod photoreceptor function.[30] As previously reported,[19] the b-wave of *Cfh*$^{-/-}$ mice was substantially attenuated compared with that of C57 mice as the flash intensity increased (Figure 3). The b-wave of *CFH-Y:Cfh*$^{-/-}$ mice was significantly larger than that of *Cfh*$^{-/-}$ mice ($P < 0.05$), particularly at higher stimulus intensities. In contrast, we were unable to detect a statistically significant rescue in the b-wave of *CFH-H:Cfh*$^{-/-}$ mice (Figure 3).

To determine whether the visual function deficit in these mice could be attributed to photoreceptor loss, we evaluated the retina structure on semithin plastic sections. We measured the extent of photoreceptor loss using measurements of ONL thickness as a function of retinal position along the superior-inferior meridian of the eye at the level of the optic nerve (Figure 4). Compared with the control C57 retina, there was an approximately 25% reduction in ONL thickness in the *Cfh*$^{-/-}$ retina. The ONL of the *CFH-Y:Cfh*$^{-/-}$ retina was significantly thicker than that of the *Cfh*$^{-/-}$ retina. In contrast, *CFH-H:Cfh*$^{-/-}$ ONL thickness showed only a slight increase over the *Cfh*$^{-/-}$ retina in the inferior portion (Figure 4). This histologic analysis suggests that attenuation of the ERGs, relative to the wild type, is most likely a reflection of the photoreceptor loss in the transgenic mice.

Human CFH Reduces the Amount of Sub-RPE Deposits

As mice age, debris accumulates between the RPE and the BrM as sub-RPE basal deposits, similar in composition to deposits seen in early AMD. We found substantial amounts of sub-RPE deposits in aged mice of all four genotypes (Figure 5). Unlike basal deposits in human tissue,[31] clear structural distinctions between basal linear deposits

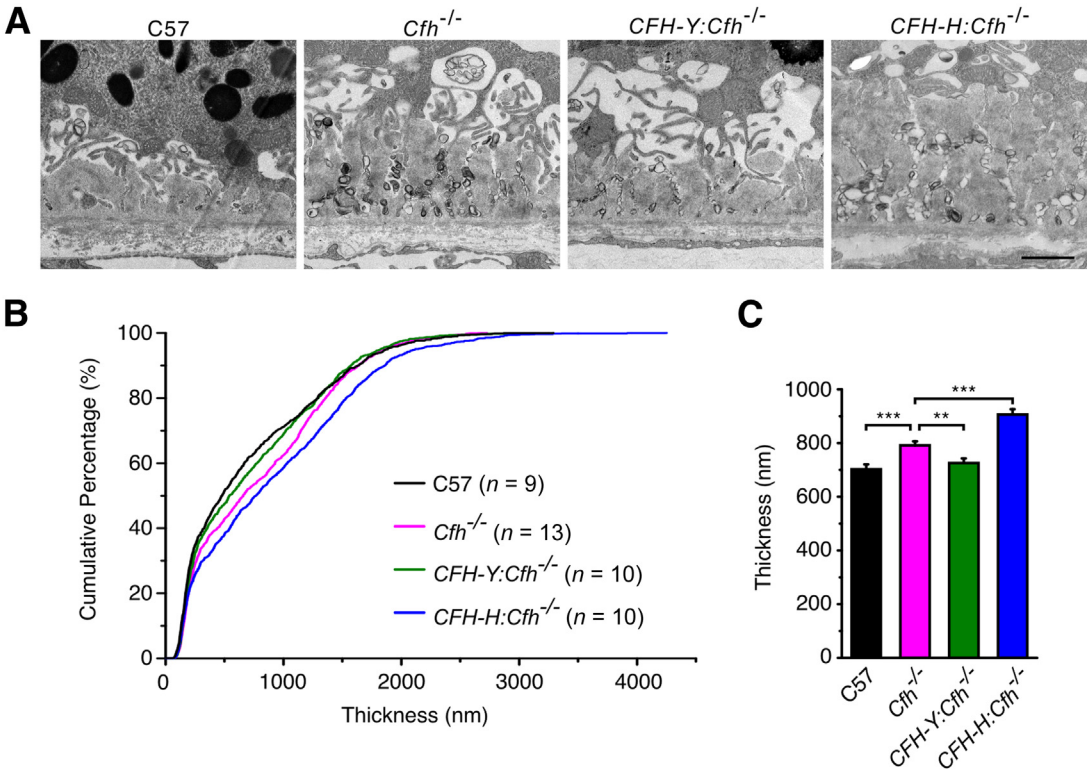

Figure 5 Expression of human CFH reduces the deposit load. **A:** Representative TEM images of basal deposits. **B:** Distribution of basal deposits for the four mouse genotypes. The genotype with the least amount of deposits is represented by the curve that is furthest left (closest to the *y* axis) in the plot (C57; black trace) compared with the curve that is furthest to the right (*CFH-H:Cfh*$^{-/-}$; blue trace) with the greatest amount of sub-RPE deposits overall. The deposit thickness was distributed over a large range for all four genotypes, but C57 mice had the least amount of basal deposits (median thickness, 321 nm). *Cfh*$^{-/-}$ mice had significantly more deposits than C57 mice (median thickness, 658 nm). The curve representing the deposit thickness in *CFH-Y:Cfh*$^{-/-}$ is close to the C57 curve, demonstrating that these mice have similar amounts of basal deposits as C57 mice (median thickness, 540 nm). The *CFH-H:Cfh*$^{-/-}$ curve, which is to the right of the *Cfh*$^{-/-}$ curve, shows that these mice had statistically significantly more deposits than *Cfh*$^{-/-}$ mice (median thickness, 763 nm). A nonparametric Kolmogorov-Smirnov test was used to compare the differences between the deposit distribution curves. **C:** The thickness of deposits. C57 and *CFH-Y:Cfh*$^{-/-}$ mice overall had fewer deposits than *Cfh*$^{-/-}$ mice, whereas *CFH-H:Cfh*$^{-/-}$ mice had the most deposits. Data are given as means ± SEM. $^{**}P < 0.01$, $^{***}P < 0.001$ (two-sample *t*-test). Scale bar = 1 μm.

(deposits within the inner collagenous layer of the BrM) and basal laminar deposits (deposits between the basal lamina of the RPE and the basal infoldings) could not be detected in mice. In fact, basal laminar deposits seemed to be the predominant form in the mice. The deposits usually had a nodular appearance, extending from the basal lamina into the spaces between the basal infoldings of the RPE. Electron-dense multilayer membranous structures of 50 to 200 nm across were frequent between nodules of deposits (Supplemental Figure S4A). These structures resembled the "membranous debris" found in the human drusen.[32] We did not notice an obvious association between the presence of the membranous debris or the long-spacing collagens and a distinct mouse genotype. The deposits were primarily amorphous, although long-spacing collagens were found in some deposits (Supplemental Figure S4B). We quantitatively measured the deposit load in the different mice to determine whether there was an increase in the amount of deposit in any of the mouse lines (Figure 5). We defined the thickness of deposits as the distance between the central elastin layer of the BrM and the basal surface of the RPE, which included basal linear and basal laminar deposits but excluded the outer collagenous layer of the BrM (Supplemental Figure S4A). The thickness of the outer collagenous layer varies depending on its spatial relationship to a nearby pillar of the choriocapillaris, but it has not been correlated to basal deposits on the RPE side of the BrM. We found that for a given retina section, the thickness of deposits varied from approximately 200 nm (no deposits) up to 4 μm (many deposits). Overall, the thickness of deposits fairly randomly distributed over the retina except where it appears to taper off nearer the ora serrata. However, in some places the thickness changes abruptly (Supplemental Figure S4, C–F). Therefore, rather than estimating the amount of sub-RPE deposits per eye by examining a few TEM images at random places, we developed a method to systematically sample and measure the thickness of sub-RPE deposits using TEM (Supplemental Figure S3; detailed in *Materials and Methods*). Using this sampling method, a means ± SD of 61 ± 8 images were taken per retina, covering nearly the entire length of a retina.

We graphed the distribution of deposit thickness on a cumulative frequency plot (Figure 5). The curve that is furthest left (closest to the *y* axis) in the plot represents the genotype with the least amount of deposits (C57, black trace) compared with the curve that is furthest to the right (*CFH-H:Cfh*$^{-/-}$, blue trace) with the greatest amount of sub-RPE deposits overall (Figure 5B). The most deposits were found in *CFH-H:Cfh*$^{-/-}$ mouse eyes. The curve for the *CFH-H:Cfh*$^{-/-}$ deposit measurements falls to the right of the *Cfh*$^{-/-}$ curve, showing that these mice had statistically

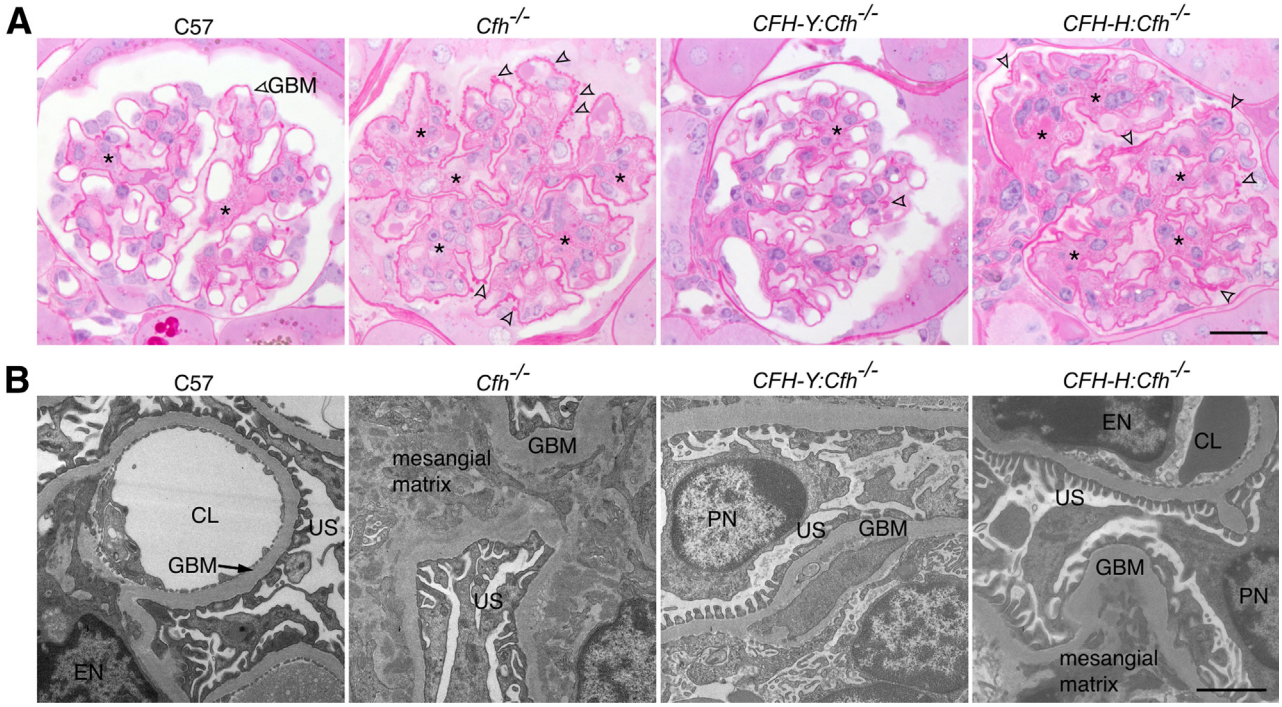

Figure 6 The human *CFH* transgene rescues kidney damage in *Cfh*$^{-/-}$ mice. **A:** Periodic acid–Schiff–stained sections of mouse kidney glomeruli. Two-year-old C57 mice showed mild age-related damage, including mild thickening of the GBM and expansion of the mesangial matrix (**asterisks**). In *Cfh*$^{-/-}$ mice, the glomerular basement membrane (GBM) was severely thickened (**arrowheads**), and the mesangial matrix was significantly expanded (**asterisks**). The structure of the *CFH-Y:Cfh*$^{-/-}$ glomerulus was similar to that of C57 mice, illustrating the protective effect of the CFH-Y transgene. In contrast, the glomeruli of the *CFH-H:Cfh*$^{-/-}$ kidneys do not show any improvement. **B:** Representative TEM images. Glomeruli of *Cfh*$^{-/-}$ and *CFH-H:Cfh*$^{-/-}$ mice showed significant thickening of the GBM and expansion of the mesangial matrix. Scale bars: 20 μm (**A**); 2 μm (**B**). CL, capillary lumen; EN, endothelial cell nucleus; PN, podocyte nucleus; US, urinary space.

Table 2 Grading of 2-Year-Old Mouse Glomerulus Pathology by Histology

C57		*Cfh*$^{-/-}$		*CFH-Y:Cfh*$^{-/-}$		*CFH-H:Cfh*$^{-/-}$	
ID	Grade	ID	Grade	ID	Grade	ID	Grade
1685	I	1549	IV	1501	I	1500	III
1686	II	1550	IV	1502	I	1547	IV
1687	II	1689	IV	1503	I	1548	IV
1688	I	1690	IV	1695	I	1693	III
				1596	I	1694	III

The glomeruli of C57 and *CFH-Y:Cfh*$^{-/-}$ mice had similar mild histologic damage (not significant; Mann-Whitney *U*-test), whereas the *Cfh*$^{-/-}$ and *CFH-H:Cfh*$^{-/-}$ glomeruli were severely damaged compared with C57 ($P < 0.05$).

significantly more deposits than *Cfh*$^{-/-}$ mice (median thickness, 763 nm). A nonparametric Kolmogorov-Smirnov test was used to compare the differences between the deposit distribution curves and for analysis of mean deposit thickness, which showed the same statistically significant differences (Student's *t*-test) (Figure 5C).

Human CFH Rescues the Renal Damage in *Cfh*$^{-/-}$ Mice

In addition to structural and functional abnormalities in the eye, *Cfh*$^{-/-}$ mice also spontaneously develop DDD. This has been attributed to uncontrolled C3 activation in these *Cfh*$^{-/-}$ mice.[21] If human CFH can inhibit mouse C3 tick-over, then we expect the kidney damage due to the *Cfh* knockout to be protected by the human protein. Thus, we examined the kidney morphology of these four lines of mice. Periodic acid–Schiff–stained kidney sections of 2-year-old C57 mice showed mild damage to the glomeruli, including slight thickening of the glomerular basement membrane (GBM) and minor expansion of the mesangial matrix (Figure 6A). Such age-related damage has been reported previously.[33] In contrast, there was much more severe damage to the glomeruli of *Cfh*$^{-/-}$ mouse kidneys, including thickening of the GBM, mesangial matrix expansion, and hypercellularity. These pathologic changes seen in *Cfh*$^{-/-}$ mice were absent in *CFH-Y:Cfh*$^{-/-}$ mice but could still be seen in *CFH-H:Cfh*$^{-/-}$ mice (Figure 6A). We also confirmed these phenotypes at the ultrastructural level (Figure 6B).

To quantify the histopathologic changes observed in the kidney, we analyzed periodic acid–Schiff–stained sections using a previously published grading method[21] in which grade 0 corresponds to normal and grade IV to most severely damaged (see *Materials and Methods* for details). The glomerular histology of C57 mice scored grades I and II, reflecting mild damage due to normal aging (Table 2). The glomeruli of *Cfh*$^{-/-}$ mice all scored grade IV, indicating the most severe damage. The glomeruli of *CFH-Y:Cfh*$^{-/-}$ mice all scored grade I, suggesting that the DDD-like pathology was inhibited by expression of the human CFH protein. However, the glomeruli in the kidneys of *CFH-H:Cfh*$^{-/-}$ mice did not show significant improvement compared with those of *Cfh*$^{-/-}$ mice (Table 2). The difference in rescue of the *Cfh*$^{-/-}$ kidney phenotype between *CFH-Y:Cfh*$^{-/-}$ and *CFH-H:Cfh*$^{-/-}$ mice suggests that there is a threshold concentration of CFH required to protect the kidney from damage, which was not reached in *CFH-H:Cfh*$^{-/-}$ mice, or that Y402 CFH is more effective at protecting the kidney than H402 CFH.

To further investigate whether the protective effect of CFH expression in *CFH-Y:Cfh*$^{-/-}$ mice was due to the inhibition of complement activation in the glomeruli by the human CFH, we immunostained for C3 and the activated C3 fragment C3b/iC3b/C3c on kidney sections (Figure 7). As expected, neither C3 nor C3b/iC3b/C3c immunolabeling was detected in C57 glomeruli, whereas immunolabeling for both was prominent in *Cfh*$^{-/-}$ glomeruli. The immunofluorescence signals in the

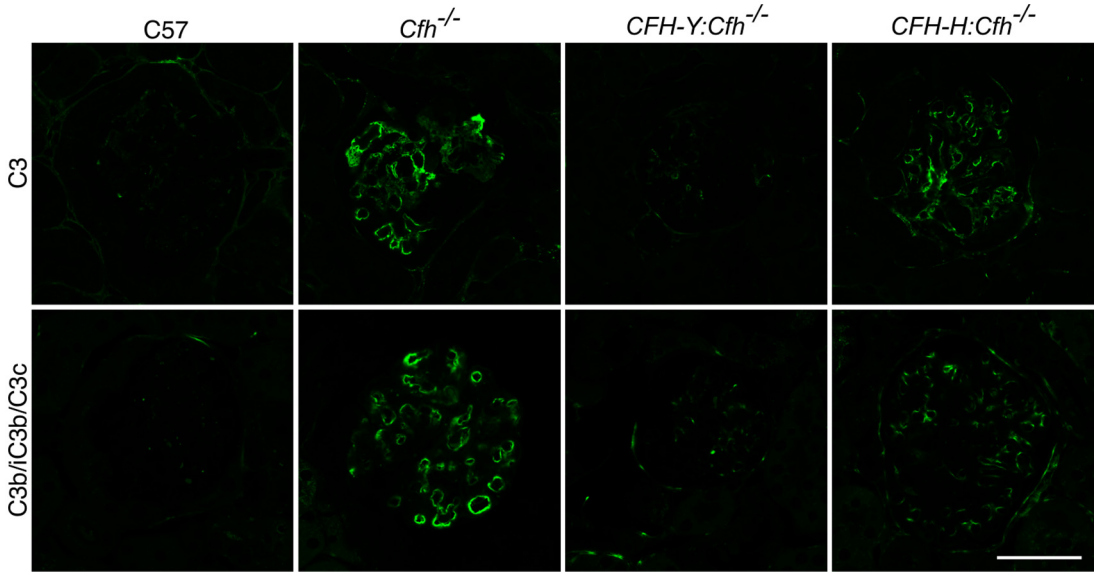

Figure 7 C3 and the activated fragment of C3, C3b/iC3b/C3c, immunofluorescence in mouse glomeruli. C3 and C3b/iC3b/C3c immunolabeling was prominent in the glomeruli of *Cfh*$^{-/-}$ and *CFH-H:Cfh*$^{-/-}$ mice but negligible in C57 and *CFH-Y:Cfh*$^{-/-}$ renal tissue. Scale bar = 50 μm.

glomeruli of *CFH-Y:Cfh*$^{-/-}$ mice were barely detectable, implying that C3 activation was inhibited. However, there were still strong C3b/iC3b/C3c labeling in the glomeruli of *CFH-H:Cfh*$^{-/-}$ mice (Figure 7).

Dose-Dependent Effects of Human CFH

So far, the results suggest that the human *CFH* transgene protected the retinal and renal damage in *CFH-Y:Cfh*$^{-/-}$ mice, but the effects were marginal or nil in *CFH-H:Cfh*$^{-/-}$ mice. Because the concentration of CFH in *CFH-Y:Cfh*$^{-/-}$ mice is twice that in *CFH-H:Cfh*$^{-/-}$ mice, it is impossible to determine whether rescue of the *Cfh*$^{-/-}$ phenotype in *CFH-Y:Cfh*$^{-/-}$ mice was due to the amount of CFH expressed or to the Y402 variant. To address this confounder, we mated *CFH-H:Cfh*$^{-/-}$ mice together to generate a line of homozygous *CFH-H* transgenic mice (*CFH-HH:Cfh*$^{-/-}$). Quantification of circulating CFH levels in *CFH-HH:Cfh*$^{-/-}$ mice revealed similar levels of CFH as *CFH-Y:Cfh*$^{-/-}$ mice (Supplemental Figure S5A). In addition, activation of the AP as measured by C3 breakdown was similar between *CFH-HH:Cfh*$^{-/-}$ and *CFH-Y:Cfh*$^{-/-}$ mice (Supplemental Figure S5B), and *CFH-HH:Cfh*$^{-/-}$ mice have the same level of hemolytic activity as *CFH-Y:Cfh*$^{-/-}$ mice (Supplemental Figure S5C).

The oldest homozygous mice examined were 8 months old at the time of the study, and they did not seem to have any obvious developmental or other abnormalities. We analyzed the retina and kidney morphology of 8-month-old mice of all the genotypes. Contrary to a previous report,[34] we did not detect any morphologic differences on semithin plastic sections between C57 and *Cfh*$^{-/-}$ mouse retinas at this age, which is consistent with the late onset of pathologic abnormalities in AMD. On the other hand, the DDD-like renal damage is detectable at this age in *Cfh*$^{-/-}$ mice (Table 3).[21] In 8-month-old *CFH-Y:Cfh*$^{-/-}$ and *CFH-HH:Cfh*$^{-/-}$ mice, the glomeruli were normal, whereas *CFH-H:Cfh*$^{-/-}$ mouse kidneys showed some damage but not to the extent detected in age-matched *Cfh*$^{-/-}$ mice (Table 3). These results demonstrate that in the kidney, the protective effects can be explained by the elevated concentration of the human CFH protein rather than the potential effect of the risk-associated H402 variant.

Table 3 Grading of 8-Month-Old Mouse Glomerulus Pathology by Histology

C57		*Cfh*$^{-/-}$		*CFH-Y:Cfh*$^{-/-}$		*CFH-H:Cfh*$^{-/-}$		*CFH-HH:Cfh*$^{-/-}$	
ID	Grade	ID	Grade	ID	Grade	ID	Grade	ID	Grade
1867	0	1870	III	1872	I	1878	II	1882	I
1868	I	1871	II	1873	0	1879	III	1883	I
1689	0	1874	III	1875	II	1881	I	1884	0
		1877	II	1876	0			1885	I
		1880	IV						

The glomeruli of C57, *CFH-Y:Cfh*$^{-/-}$, and *CFH-HH:Cfh*$^{-/-}$ mice were normal at 8 months, whereas the *Cfh*$^{-/-}$ and *CFH-H:Cfh*$^{-/-}$ glomeruli were damaged compared with C57 ($P < 0.05$).

Discussion

AMD and DDD share the H402 at-risk genotype as well as overt pathologic similarities supporting the existence of a genotype-phenotype relationship.[14] We generated transgenic mice that express the normal or risk-associated variants of the full-length human CFH protein. For the first time, we show that human CFH prevents the retina and kidney damage caused by *Cfh* deletion in a dose-dependent manner and that human CFH can inhibit the mouse AP of the complement system *in vivo*.

CFH is a large soluble glycoprotein of 155 kDa that consists of 20 short consensus repeats (SCR). The H402 variant associated with risk of AMD and DDD is located in SCR7. Previously, transgenic mice expressing a chimeric CFH, in which the human CFH sequence for SCR6-8 flanked by mouse sequences SCR1-5 and SCR9-20, were generated.[35] Despite the fact that the chimeric CFH protein expressed in these animals could restore the C3 serum levels of *Cfh*$^{-/-}$ mice, they still developed early AMD-like pathologic abnormalities at as young as 12 months old, an age at which the retina of *Cfh*$^{-/-}$ mice is still relatively normal. Thus, it is possible that the effect of the expressed chimeric protein is unrelated to modulation of the AP. Expression of the chimeric protein in these animals is controlled by an apolipoprotein E promoter.[35] Apolipoprotein E is expressed in the RPE, but it is also expressed by Müller cells in the neural retina.[36] Therefore, it is plausible that the chimeric CFH produced by Müller cells exerts adverse effects on the structure and function of the retina unrelated to modulation of the AP. In contrast, the full-length BACs we used to create the humanized CFH mice include the endogenous regulatory elements in the transgene, which allows normal tissue- and cell-specific expression of human CFH. This is especially important in the case of *CFH*, which is a large, complex gene with many introns and exons and alternative splicing. Furthermore, once a gene expression pattern is recapitulated by a BAC transgene (which we show in the present study), the regulatory elements that are crucial to gene regulation, RNA processing, and other operations may potentially be systematically dissected in a way that is not possible in humans.[37,38]

Human and mouse CFH proteins share 61% identity and 70% similarity. Mouse CFH is 1252 amino acids in length compared with human CFH, which is 1231 amino acids, and it is less glycosylated than the human form. It was, therefore, not self-evident that human CFH could function properly in the mouse complement system. This study established that human CFH can, in fact, effectively regulate the mouse AP. The protection from damage in the eye associated with *Cfh*$^{-/-}$ in these humanized mice was directly correlated with the human CFH levels expressed in each line. These findings are consistent with a recent population study showing that some AMD patients have decreased plasma CFH concentrations.[39] Still, it cannot be entirely ruled out that the phenotypic differences we have

seen between *CFH-H:Cfh*$^{-/-}$ and *CFH-Y:Cfh*$^{-/-}$ mice could be due to the H versus Y amino acid at position 402.

Cells in the RPE/choroid/sclera of C57, *CFH-H:Cfh*$^{-/-}$, and *CFH-Y:Cfh*$^{-/-}$ mice synthesize C3, CFH, and FB, whereas *Cfh*$^{-/-}$ mice synthesize C3 and FB. The contribution in the eye of these locally produced complement proteins compared with the contribution of complement proteins from the circulation is not known; however, this study indicates that there was a smaller difference in the relative amounts of C3 and C3b between genotypes in the RPE/choroid/sclera. In fact, a small amount of intact C3 was detected in *Cfh*$^{-/-}$ mice in the RPE/choroid/sclera, suggesting that inhibitors other than CFH act on locally produced C3 (Figure 2B). These are likely to be the membrane-bound inhibitors of complement (Crry, CD55, and CD46).

Since discovery of the genetic association between *CFH* and AMD, one of the major tasks has been to explore the functional differences between normal Y402 and risk-associated H402 variants of CFH. A few *in vitro* studies using recombinant CFH or fragments containing SCR7 have reported functional differences between the Y402 and H402 variants.[40,41] In contrast, our previous work using full-length proteins extracted from human plasma demonstrated that the two variants were indistinguishable in fluid-phase functional assays.[25] These results highlight the complexity of the CFH molecule and the important differences between native full-length CFH and recombinant fragments or full-length proteins. For example, dependence on the tertiary structure and interaction of different regions of the CFH molecule for binding and activity cannot be entirely replicated by recombinant fragments of CFH.

One of the primary purposes of creating humanized CFH mice was to investigate the functional differences between the CFH variants in a well-controlled model system. However, this goal was hampered by the difference in expression levels of the CFH protein in the two mouse lines. To address this problem and match the protein levels between the variants we generated a homozygous *CFH-H* transgenic mouse line crossed to the *Cfh*$^{-/-}$, which has twice the concentration of hemizygous *CFH-H:Cfh*$^{-/-}$ and is, thus, expressed at levels similar to *CFH-Y:Cfh*$^{-/-}$. Initial analysis of the kidneys of young mice showed no differences between *CFH-HH:Cfh*$^{-/-}$ and *CFH-Y:Cfh*$^{-/-}$ mice. In future studies, we still need to examine the ocular phenotype in these *CFH-HH:Cfh*$^{-/-}$ mice when they are old enough (2 years) to determine whether their eyes are also similar to those of *CFH-Y:Cfh*$^{-/-}$ mice because characterizing the *CFH-HH:Cfh*$^{-/-}$ mice will determine whether the findings described herein are solely due to concentration effects or whether the CFH genotype plays a role in the observed pathologic abnormality.

We will be particularly interested in analyzing the levels of the sub-RPE deposit in *CFH-HH:Cfh*$^{-/-}$ mice because unlike the other ocular phenotypes associated with *Cfh*$^{-/-}$, the amount of basal deposits in hemizygous *CFH-H:Cfh*$^{-/-}$ mice were not decreased compared with the amounts in *Cfh*$^{-/-}$ but rather were increased even more than that in *Cfh*$^{-/-}$ mice. The presence of statistically significantly thicker sub-RPE deposits compared with deposits in *Cfh*$^{-/-}$ mice combined with apparent protection in the neural retina in *CFH-H:Cfh*$^{-/-}$ mice, based on ONL thickness, compared with *Cfh*$^{-/-}$ mice suggests that the events in neural retina and RPE/choroid are separable. The H variant of CFH may increase the risk of AMD by facilitating more sub-RPE deposit formation without directly contributing to damaging the neural retina.

CFH deficiency causes DDD, atypical hemolytic-uremic syndrome, and other renal diseases. There is no definitive therapy for DDD,[42] although a single dose of human CFH injected into *Cfh*$^{-/-}$ mice can briefly restore serum C3 levels and resolve GBM C3 deposition.[43] This finding supported the use of exogenous human CFH as a potential new therapy for patients with DDD or atypical hemolytic-uremic syndrome associated with CFH deficiency. However, preclinical tests in *Cfh*$^{-/-}$ mice with long-term administration of human CFH were inconclusive as the mice eventually generated anti-human CFH antibodies that triggered immune complex glomerulonephritis and renal failure.[43] The *CFH-H:Cfh*$^{-/-}$ mice characterized in the present study represent a good model to test human CFH therapy for DDD because these mice have detectable levels of human CFH and are, thus, unlikely to generate anti-human CFH antibodies when human CFH is administered, but they also still develop the DDD-like phenotype needed to test potential therapies.

In conclusion, we developed new murine models expressing normal and variants of human CFH associated with risk of AMD and DDD. Analysis of these animals revealed, for the first time, that human CFH can inhibit the mouse AP *in vivo*. In addition, we show that human CFH prevents the retina and kidney damage caused by *Cfh* deletion in a dose-dependent manner. The animal models represent valuable tools to study the mechanisms and environmental contributors of normal and at-risk human CFH variants in a defined model system.

Acknowledgments

We thank Dr. Nikolai Skiba for assistance with human CFH peptide identification by MALDI, Dr. Marina Botto for access to *Cfh*$^{-/-}$ mice, Dr. Dan Stamer for critical comments on the manuscript, and Drs. Bernd Gloss and Ute Hochgeschwender (Duke Neurotransgenic Laboratory) for excellent technical support.

Supplemental Data

Supplemental material for this article can be found at *http://dx.doi.org/10.1016/j.ajpath.2014.08.026*.

References

1. Friedman DS, O'Colmain BJ, Munoz B, Tomany SC, McCarty C, de Jong PT, Nemesure B, Mitchell P, Kempen J; Eye Diseases Prevalence

Research Group: Prevalence of age-related macular degeneration in the United States. Arch Ophthalmol 2004, 122:564–572
2. Klein R, Peto T, Bird A, Vannewkirk MR: The epidemiology of age-related macular degeneration. Am J Ophthalmol 2004, 137:486–495
3. Bowes Rickman C, Farsiu S, Toth CA, Klingeborn M: Dry age-related macular degeneration: mechanisms, therapeutic targets, and imaging. Invest Ophthalmol Vis Sci 2013, 54:ORSF68–ORSF80
4. Jager RD, Mieler WF, Miller JW: Age-related macular degeneration. N Engl J Med 2008, 358:2606–2617
5. de Jong PT: Age-related macular degeneration. N Engl J Med 2006, 355:1474–1485
6. Jackson GR, Owsley C, McGwin G Jr: Aging and dark adaptation. Vision Res 1999, 39:3975–3982
7. Jackson GR, McGwin G Jr, Phillips JM, Klein R, Owsley C: Impact of aging and age-related maculopathy on activation of the a-wave of the rod-mediated electroretinogram. Invest Ophthalmol Vis Sci 2004, 45: 3271–3278
8. Age-Related Eye Disease Study Research Group: Risk factors associated with age-related macular degeneration. a case-control study in the age-related eye disease study: Age-Related Eye Disease Study Report Number 3. Ophthalmology 2000, 107:2224–2232
9. Edwards AO, Ritter R III, Abel KJ, Manning A, Panhuysen C, Farrer LA: Complement factor H polymorphism and age-related macular degeneration. Science 2005, 308:421–424
10. Hageman GS, Anderson DH, Johnson LV, Hancox LS, Taiber AJ, Hardisty LI, Hageman JL, Stockman HA, Borchardt JD, Gehrs KM, Smith RJ, Silvestri G, Russell SR, Klaver CC, Barbazetto I, Chang S, Yannuzzi LA, Barile GR, Merriam JC, Smith RT, Olsh AK, Bergeron J, Zernant J, Merriam JE, Gold B, Dean M, Allikmets R: A common haplotype in the complement regulatory gene factor H (HF1/CFH) predisposes individuals to age-related macular degeneration. Proc Natl Acad Sci U S A 2005, 102:7227–7232
11. Haines JL, Hauser MA, Schmidt S, Scott WK, Olson LM, Gallins P, Spencer KL, Kwan SY, Noureddine M, Gilbert JR, Schnetz-Boutaud N, Agarwal A, Postel EA, Pericak-Vance MA: Complement factor H variant increases the risk of age-related macular degeneration. Science 2005, 308:419–421
12. Klein RJ, Zeiss C, Chew EY, Tsai JY, Sackler RS, Haynes C, Henning AK, SanGiovanni JP, Mane SM, Mayne ST, Bracken MB, Ferris FL, Ott J, Barnstable C, Hoh J: Complement factor H polymorphism in age-related macular degeneration. Science 2005, 308: 385–389
13. Abrera-Abeleda MA, Nishimura C, Smith JL, Sethi S, McRae JL, Murphy BF, Silvestri G, Skerka C, Jozsi M, Zipfel PF, Hageman GS, Smith RJ: Variations in the complement regulatory genes factor H (CFH) and factor H related 5 (CFHR5) are associated with membranoproliferative glomerulonephritis type II (dense deposit disease). J Med Genet 2006, 43:582–589
14. Pickering MC, de Jorge EG, Martinez-Barricarte R, Recalde S, Garcia-Layana A, Rose KL, Moss J, Walport MJ, Cook HT, de Cordoba SR, Botto M: Spontaneous hemolytic uremic syndrome triggered by complement factor H lacking surface recognition domains. J Exp Med 2007, 204:1249–1256
15. Appel GB, Cook HT, Hageman G, Jennette JC, Kashgarian M, Kirschfink M, Lambris JD, Lanning L, Lutz HU, Meri S, Rose NR, Salant DJ, Sethi S, Smith RJ, Smoyer W, Tully HF, Tully SP, Walker P, Welsh M, Wurzner R, Zipfel PF: Membranoproliferative glomerulonephritis type II (dense deposit disease): an update. J Am Soc Nephrol 2005, 16:1392–1403
16. Walker PD: Dense deposit disease: new insights. Curr Opin Nephrol Hypertens 2007, 16:204–212
17. Morgan BP, Harris CL: Complement Regulatory Proteins. San Diego, Academic Press, 1999
18. Holers VM: The spectrum of complement alternative pathway-mediated diseases. Immunol Rev 2008, 223:300–316
19. Coffey PJ, Gias C, McDermott CJ, Lundh P, Pickering MC, Sethi C, Bird A, Fitzke FW, Maass A, Chen LL, Holder GE, Luthert PJ, Salt TE, Moss SE, Greenwood J: Complement factor H deficiency in aged mice causes retinal abnormalities and visual dysfunction. Proc Natl Acad Sci U S A 2007, 104:16651–16656
20. Hoh Kam J, Lenassi E, Malik TH, Pickering MC, Jeffery G: Complement component C3 plays a critical role in protecting the aging retina in a murine model of age-related macular degeneration. Am J Pathol 2013, 183:480–492
21. Pickering MC, Cook HT, Warren J, Bygrave AE, Moss J, Walport MJ, Botto M: Uncontrolled C3 activation causes membranoproliferative glomerulonephritis in mice deficient in complement factor H. Nat Genet 2002, 31:424–428
22. Meisler MH: Insertional mutation of 'classical' and novel genes in transgenic mice. Trends Genet 1992, 8:341–344
23. Mattapallil MJ, Wawrousek EF, Chan CC, Zhao H, Roychoudhury J, Ferguson TA, Caspi RR: The Rd8 mutation of the Crb1 gene is present in vendor lines of C57BL/6N mice and embryonic stem cells, and confounds ocular induced mutant phenotypes. Invest Ophthalmol Vis Sci 2012, 53:2921–2927
24. Livak KJ, Schmittgen TD: Analysis of relative gene expression data using real-time quantitative PCR and the 2(-Delta Delta C(T)) Method. Methods 2001, 25:402–408
25. Kelly U, Yu L, Kumar P, Ding JD, Jiang H, Hageman GS, Arshavsky VY, Frank MM, Hauser MA, Bowes Rickman C: Heparan sulfate, including that in Bruch's membrane, inhibits the complement alternative pathway: implications for age-related macular degeneration. J Immunol 2010, 185:5486–5494
26. Ding JD, Johnson LV, Herrmann R, Farsiu S, Smith SG, Groelle M, Mace BE, Sullivan P, Jamison JA, Kelly U, Harrabi O, Bollini SS, Dilley J, Kobayashi D, Kuang B, Li W, Pons J, Lin JC, Bowes Rickman C: Anti-amyloid therapy protects against retinal pigmented epithelium damage and vision loss in a model of age-related macular degeneration. Proc Natl Acad Sci U S A 2011, 108:E279–E287
27. Ding JD, Lin J, Mace BE, Herrmann R, Sullivan P, Bowes Rickman C: Targeting age-related macular degeneration with Alzheimer's disease based immunotherapies: anti-amyloid-beta antibody attenuates pathologies in an age-related macular degeneration mouse model. Vision Res 2008, 48:339–345
28. Herrmann R, Lobanova ES, Hammond T, Kessler C, Burns ME, Frishman LJ, Arshavsky VY: Phosducin regulates transmission at the photoreceptor-to-ON-bipolar cell synapse. J Neurosci 2010, 30: 3239–3253
29. Kelly U, Bowes Rickman C, Postel EA, Hauser MA, Hageman GS, Arshavsky VY, Skiba NP: Rapid and sensitive method for detection of Y402, H402, I62, and V62 variants of complement factor H in human plasma samples using mass spectrometry. Invest Ophthalmol Vis Sci 2009, 50:1540–1545
30. Gouras P: Electroretinography: some basic principles. Invest Ophthalmol 1970, 9:557–569
31. Johnson M, Dabholkar A, Huang JD, Presley JB, Chimento MF, Curcio CA: Comparison of morphology of human macular and peripheral Bruch's membrane in older eyes. Curr Eye Res 2007, 32: 791–799
32. Curcio CA, Presley JB, Millican CL, Medeiros NE: Basal deposits and drusen in eyes with age-related maculopathy: evidence for solid lipid particles. Experimental Eye Research 2005, 80:761–775
33. Lim JH, Kim EN, Kim MY, Chung S, Shin SJ, Kim HW, Yang CW, Kim YS, Chang YS, Park CW, Choi BS: Age-associated molecular changes in the kidney in aged mice. Oxid Med Cell Longev 2012, 2012:171383
34. Williams JA, Greenwood J, Moss SE: Retinal changes precede visual dysfunction in the complement factor H knockout mouse. PLoS One 2013, 8:e68616
35. Ufret-Vincenty RL, Aredo B, Liu X, McMahon A, Chen PW, Sun H, Niederkorn JY, Kedzierski W: Transgenic mice expressing variants of complement factor H develop AMD-like retinal findings. Invest Ophthalmol Vis Sci 2010, 51:5878–5887

36. Amaratunga A, Abraham CR, Edwards RB, Sandell JH, Schreiber BM, Fine RE: Apolipoprotein E is synthesized in the retina by Muller glial cells, secreted into the vitreous, and rapidly transported into the optic nerve by retinal ganglion cells. J Biol Chem 1996, 271:5628–5632
37. Yu W, Misulovin Z, Suh H, Hardy RR, Jankovic M, Yannoutsos N, Nussenzweig MC: Coordinate regulation of RAG1 and RAG2 by cell type-specific DNA elements 5′ of RAG2. Science 1999, 285: 1080–1084
38. Yang XW, Gong S: An overview on the generation of BAC transgenic mice for neuroscience research. Curr Protoc Neurosci 2005, Chapter 5. Unit 5.20
39. Ansari M, McKeigue PM, Skerka C, Hayward C, Rudan I, Vitart V, Polasek O, Armbrecht AM, Yates JR, Vatavuk Z, Bencic G, Kolcic I, Oostra BA, Van Duijn CM, Campbell S, Stanton CM, Huffman J, Shu X, Khan JC, Shahid H, Harding SP, Bishop PN, Deary IJ, Moore AT, Dhillon B, Rudan P, Zipfel PF, Sim RB, Hastie ND, Campbell H, Wright AF: Genetic influences on plasma CFH and CFHR1 concentrations and their role in susceptibility to age-related macular degeneration. Hum Mol Genet 2013, 22:4857–4869
40. Clark SJ, Perveen R, Hakobyan S, Morgan BP, Sim RB, Bishop PN, Day AJ: Impaired binding of the age-related macular degeneration-associated complement factor H 402H allotype to Bruch's membrane in human retina. J Biol Chem 2010, 285:30192–30202
41. Prosser BE, Johnson S, Roversi P, Herbert AP, Blaum BS, Tyrrell J, Jowitt TA, Clark SJ, Tarelli E, Uhrin D, Barlow PN, Sim RB, Day AJ, Lea SM: Structural basis for complement factor H linked age-related macular degeneration. J Exp Med 2007, 204:2277–2283
42. Smith RJ, Alexander J, Barlow PN, Botto M, Cassavant TL, Cook HT, de Cordoba SR, Hageman GS, Jokiranta TS, Kimberling WJ, Lambris JD, Lanning LD, Levidiotis V, Licht C, Lutz HU, Meri S, Pickering MC, Quigg RJ, Rops AL, Salant DJ, Sethi S, Thurman JM, Tully HF, Tully SP, van der Vlag J, Walker PD, Wurzner R, Zipfel PF; Dense Deposit Disease Focus Group: New approaches to the treatment of dense deposit disease. J Am Soc Nephrol 2007, 18:2447–2456
43. Fakhouri F, de Jorge EG, Brune F, Azam P, Cook HT, Pickering MC: Treatment with human complement factor H rapidly reverses renal complement deposition in factor H-deficient mice. Kidney Int 2010, 78:279–286